SIN-CHN SCIENTIFIC PRESS PTE.LTD.

Molecular & Cellular Biomechanics 2025, 22(2), 1245.
https://doi.org/10.62617/mcb1245

Article

Biometric recognition and analysis of sports teaching behavior based on wearable devices

Hui Ma[1], Xuelian Ma[2,*]

[1] Hebei Agricultural University, Baoding 071051, China
[2] Hebei Vocational University of Technology and Engineering, Xingtai 054000, China
*** Corresponding author:** Xuelian Ma, maxiaoxiaoxiao666@126.com

CITATION

Ma H, Ma X. Biometric recognition and analysis of sports teaching behavior based on wearable devices. Molecular & Cellular Biomechanics. 2025; 22(2): 1245. https://doi.org/10.62617/mcb1245

ARTICLE INFO

Received: 24 December 2024
Accepted: 31 December 2024
Available online: 16 January 2025

Abstract: This study introduces a lightweight, multi-node IMU-based motion capture system optimized for biomechanical analysis, addressing limitations of traditional optical systems and challenges in sensor drift and noise. Multi-node IMU systems offer distinct advantages in biomechanical analysis, such as portability, affordability, and the ability to capture motion data in real-world environments, making them particularly suited for applications in gait analysis, sports performance, and rehabilitation. Enhanced calibration techniques correct biases in accelerometers, gyroscopes, and magnetometers, while an optimized Madgwick algorithm ensures accurate, real-time motion tracking. The system's scalable design, supported by high-throughput USB 3.0 communication, enables precise capture of human motion. Experimental validation confirms the system's affordability, robustness, and suitability for biomechanics, offering a practical and effective tool for advancing human movement research.

Keywords: biomechanics; motion capture; IMU sensors; physical education; gait analysis; sports performance; rehabilitation; human movement; scalable system design

1. Introduction

The study of biomechanics, which examines the mechanical principles of human movement, plays a pivotal role in understanding physical performance, preventing injuries, and developing effective rehabilitation strategies. By analyzing how forces interact with the human body, biomechanics provides valuable insights into muscle dynamics, joint movements, and overall kinematics [1–3]. However, accurate data acquisition remains a challenge, often requiring sophisticated and precise motion capture systems to study complex human movements in real-world scenarios.

Traditional optical-based motion capture systems have been widely used in biomechanics for their high accuracy and ability to deliver detailed three-dimensional motion data [4,5]. These systems use cameras and markers to track body movements, making them invaluable for applications such as gait analysis, sports performance optimization, and clinical studies. However, their dependence on controlled environments, high cost, complex installation, and limited portability restrict their usability in dynamic, outdoor, or resource-constrained settings. These limitations create a demand for more accessible, flexible, and cost-effective motion capture solutions for biomechanical research and applications [6,7].

Inertial Measurement Unit (IMU)-based systems have emerged as a promising alternative for motion capture in biomechanics. These systems use accelerometers, gyroscopes, and magnetometers to measure linear acceleration, angular velocity, and magnetic field strength, enabling detailed tracking of body movements without

reliance on external infrastructure [8,9]. Their portability, lower cost, and ease of deployment make them ideal for studying biomechanics in diverse settings, including sports fields, clinics, and rehabilitation centers. Despite these advantages, IMU-based systems face challenges such as sensor noise, drift, and interference from environmental factors, which can reduce the accuracy of motion data critical for biomechanical analysis [10]. Overcoming these challenges to deliver high-quality motion capture data for biomechanics is an ongoing area of research.

This paper addresses these challenges by proposing a lightweight, multi-node motion capture system based on IMU sensors, designed specifically for biomechanical applications. The system combines advanced sensor calibration techniques with a refined data fusion algorithm to improve the accuracy and reliability of motion capture data. Static and dynamic calibration methods are applied to correct biases in accelerometers, gyroscopes, and magnetometers, ensuring precise measurements critical for biomechanical studies [11]. The motion capture system also integrates an optimized Madgwick filter with adaptive step-size adjustments to enhance real-time tracking and reduce sensor drift, making it suitable for capturing dynamic movements with high fidelity. Furthermore, the system incorporates a scalable, USB 3.0-based communication framework, enabling multi-node configurations that are essential for capturing full-body motion in complex biomechanical analyses.

By focusing on the needs of biomechanics, the proposed system offers several significant advantages. It supports precise gait analysis, enabling researchers and clinicians to evaluate walking patterns, identify abnormalities, and design targeted rehabilitation programs. The system's portability and cost-effectiveness make it particularly valuable for sports performance analysis, where tracking movements in real-world conditions is critical. Additionally, its robustness against noise and environmental interference ensures reliable data collection for rehabilitation monitoring, allowing healthcare professionals to assess recovery progress with confidence [12].

This work contributes to the field of biomechanics by providing an accessible, accurate, and scalable tool for studying human movement. By bridging the gap between traditional optical systems and portable IMU-based alternatives, the proposed motion capture system enhances the ability of researchers, clinicians, and practitioners to analyze human motion in diverse and dynamic environments. Through extensive experimental validation, this study demonstrates the system's potential to advance biomechanics research and practical applications in sports, rehabilitation, and human performance optimization.

2. Related work

The United States started investigating elementary physical education as early as 1997, which is when overseas online physical education first got underway. As we enter the twenty-first century, remote education has grown quickly. In the United States, 700,000 students were enrolled in online K–12 instruction in 2004–2005, and by 2009, that figure had risen to over 1 million [13]. Online sports in other nations have progressively reduced the issue of unequal distribution of sports resources and produced certain outcomes via constant research and practice.

After decades of development, China has progressively covered nearly all pertinent areas in the field of sensor technology, having started conducting extensive research on the subject in the early 1990s [14]. Despite its high accuracy, the traditional multi-sensor technology's use is restricted by its large size, heavy weight, and lengthy initial calibration period [15]. It is primarily utilized in the fields of navigation, aerospace, and land navigation for military vehicles. Since MEMS technology has advanced so quickly, multi-sensors are becoming the best choice for data collecting modules in motion capture systems due to their lower cost, smaller size, reduced power consumption, and noticeable gains in accuracy and integration. **Figure 1** depicts the outside of the Xsens MVN motion capture system.

Figure 1. Motion capture system Xsens MVN.

The SharkStream motion capture system, which was unveiled at the World Consumer Electronics Show (CES) in Las Vegas, uses two antennas to wirelessly broadcast across a distance of more than 250 m and has a one-day battery life. The technology makes use of a communication protocol that was created internally and has better algorithmic accuracy. The Perception Neuron from Noitom is the most reasonably priced, portable, and versatile high-performance motion capture device available, as seen in **Figure 2**. It is also the world's most user-friendly motion capture technology, achieving smoother and more realistic trajectory replication due to its high precision and low latency.

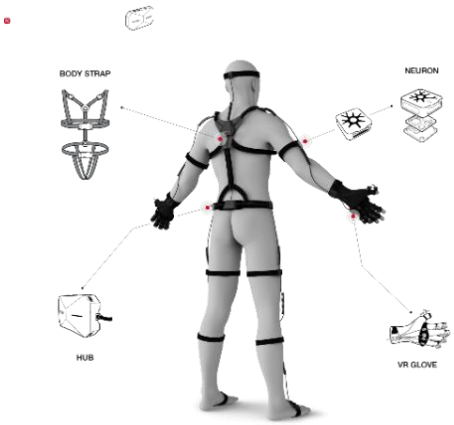

Figure 2. Motion capture system for Noitom perception neurons.

3. Design of the system

In order to map any movement of the actual human body to the host computer's 3D character model, the goal of this article is to design a multi-sensor based online sports motion capture system that can achieve whole body motion tracking. Modules for data collecting, communication, processing, and recovery make up the majority of the system. By merging the current motion capture algorithms and architectures, the objective is to create an inertial online motion capture system that can record the movement of the entire body in real time. **Figure 3** depicts the system architecture.

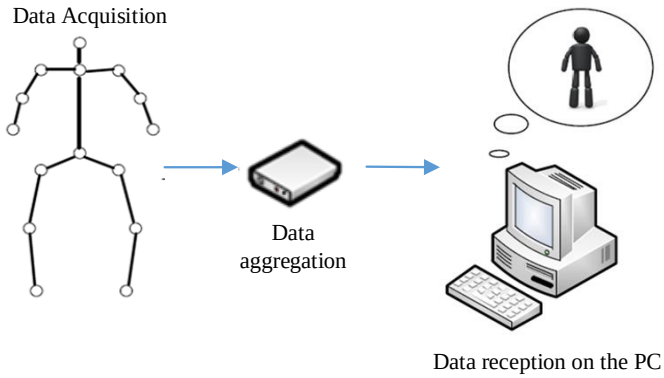

Figure 3. Architecture of a full-body motion capture system for online physical education.

The sensor is a mechanical device that is susceptible to interference due to its nature and design philosophy. Additionally, the PCB components cannot be attached in a way that keeps the sensor level with the PCB board. This leads to inevitable errors that could lead to the sensor drifting to zero. As a result, the elliptical fitting approach is used to calibrate the magnetometer, gyroscope, and accelerometer.

3.1. Calibration of an accelerometer

The three types of accelerometer sensors are thermal inductive, capacitive, and piezoelectric. They are further divided into single-, dual-, and tri-axis types based on the number of input axes. Because of their small size and low weight, they can assess spatial acceleration and accurately depict object motion, making them widely used in robotics, automotive, and aerospace applications. Attitude monitoring also makes extensive use of inexpensive three-axis accelerometers. However, mistakes brought on by welding attachment can reduce measurement accuracy. For this reason, by eliminating measurement errors caused by problems such as the coordinate axes of triaxial accelerometers not being perpendicular, calibrating the accelerometers enhances data reliability.

Method for calibrating gravity references

The second non-instrumentation calibration approach, the gravity reference calibration method, was chosen for this paper. When the accelerometer is positioned statically, the observed value should, in theory, always be the local gravity acceleration. The local acceleration of gravity in the component's three dimensions

should now be measured by the accelerometer's three axes; this can be done using the vector technique, as Equation (1) illustrates.

$$acc_x^2 + acc_y^2 + acc_z^2 = G^2 \tag{1}$$

$$\begin{bmatrix} D_x \\ D_y \\ D_z \end{bmatrix} = \begin{bmatrix} S_x & k_{xy} & k_{xz} \\ k_{yx} & S_y & k_{yz} \\ k_{zx} & k_{zy} & S_z \end{bmatrix} \begin{bmatrix} M_x \\ M_y \\ M_z \end{bmatrix} + \begin{bmatrix} B_x \\ B_y \\ B_z \end{bmatrix} \tag{2}$$

$$\begin{bmatrix} D_x \\ D_y \\ D_z \end{bmatrix} = \begin{bmatrix} S_x & 0 & 0 \\ 0 & S_y & 0 \\ 0 & 0 & S_z \end{bmatrix} \begin{bmatrix} M_x \\ M_y \\ M_z \end{bmatrix} + \begin{bmatrix} B_x \\ B_y \\ B_z \end{bmatrix} \tag{3}$$

$$D = \begin{bmatrix} b & 0 & 0 \\ -b & 0 & 0 \\ 0 & b & 0 \\ 0 & -b & 0 \\ 0 & 0 & b \\ 0 & 0 & -b \end{bmatrix} \tag{4}$$

The offset of each axis is then obtained by averaging the greatest and minimum gravitational acceleration measurements on each axis, as indicated by Equation (5).

$$B = \frac{M_{\max} + M_{\min}}{2} \tag{5}$$

The calibration of the accelerometer is completed by solving the linear equation system by integrating the actual recorded acceleration *M* and Equations (4) and (5) into the measurement model Equation (3). Since the accelerometer's inaccuracy depends only on the device's features, it is frequently calibrated just once.

3.2. Gyroscope adjustment

Gyroscopes measure the angle between the internal rotor's vertical axis and the carrier to determine angular velocity. Three mutually perpendicular single-axis gyroscopes make up the three-axis gyroscope, which can determine the carrier's motion in three dimensions based on its angle and angular velocity but not its geographic direction. Its measurement precision has a direct impact on the system attitude resolution because it is the primary component of the online sports motion capture system. Gyroscopes must be recalibrated after every power-up to guarantee optimal operation because they are sensitive to environmental factors, particularly temperature [2].

Method of field calibration

The gyroscope's mathematical model is established by Equation (6).

$$\begin{bmatrix} G_x \\ G_y \\ G_z \end{bmatrix} = \begin{bmatrix} g_{0x} \\ g_{0y} \\ g_{0z} \end{bmatrix} + \begin{bmatrix} g_x \\ g_y \\ g_z \end{bmatrix} + \begin{bmatrix} v_{gx} \\ v_{gy} \\ v_{gz} \end{bmatrix} \tag{6}$$

As the temperature changes, the gyroscope will experience zero point drift. Therefore, the primary goal of gyroscope calibration is to rectify the zero bias in comparison to the zero bias, ignoring the little amount of random error.

$$\omega_c = \frac{1}{k}\left[\sum_{i=1}^{k} \omega_i\right] \tag{7}$$

3.3. Calibration of magnetometers

From the magnetic south pole to the magnetic north pole, the earth's magnetic field is a vector field. However, the direct use of a magnetometer may result in significant mistakes due to the nature of the apparatus and its sensitivity to disturbances in the surrounding magnetic field; therefore, error correction of the magnetometer is necessary to increase the measurement accuracy.

The magnetometer uses the known gravitational magnetic field of Earth to calculate its three-dimensional spatial position by measuring the angle between the carrier and the magnetic field. In principle, the magnetometer's X, Y, and Z axes ought should be perpendicular to each other. When the sensor is rotated, the trajectory of the measured value should form a three-dimensional sphere with the origin as the center and the local magnetic field strength as the radius, provided that the environmental circumstances remain constant. But in practice, factors like zero bias and three-axis non-orthogonality affect the magnetometer and lead to errors. As Equation (8) shows, this necessitates the creation of a mathematical model of the magnetometer.

$$M = mag_{offs} + m + v_m \tag{8}$$

$$mag_{offs} = \frac{mag_{\max} + mag_{\min}}{2} \tag{9}$$

The magnetometer is calibrated by subtracting the data for each axis from the corresponding X-, Y-, and Z-axis offsets after the offset determined by Equation (9) has been entered into the mathematical model of the magnetometer. The magnetometer and accelerometer are calibrated in the same way. The calibration is only required once if there is no discernible magnetic interference.

4. Data collect

A total of 608 individuals were surveyed, with 587 questionnaires collected, of which 514 were valid (an effective rate of 87.6%) and 73 were invalid. The main reasons for invalid responses included incomplete questionnaires (62) and inconsistencies (11). Among the valid responses, 394 were male and 120 were female, with a male-to-female ratio of 3.28:1. The average age of respondents was 40.25 years. The largest age group was 36–45 years (24.9%), followed by 26–35 years (21.4%), under 25 years (19.5%), and 56–69 years (10.7%).

Regarding education, 46% had a junior high school education, 19.7% had a high school or vocational school education, 13.6% had primary school education, 16.8% were college students, and 8.4% were illiterate or had limited literacy. Most respondents were of Han ethnicity (93.25%), with 1.9% Hui and 4.9% from other ethnicities. Marital status showed that 80.2% were married, 15.6% were unmarried, and 4.3% were widowed or divorced.

Table 1. Demographic characteristics of respondents (N = 514).

Demographic characteristics	**Number of respondents (*n*)**	**Composition ratio (%)**
Gender		
Male	394	76.5
Female	120	23.5
Age (years)		
≤ 26	100	19.7
27–36	110	21.5
37–46	128	24.8
47–56	121	23.7
57–70	55	10.5
Nation		
Han nationality	479	93.5
Hui nationality	10	2.1
Other	25	4.8
Degree of education		
Illiterate or illiterate	43	8.6
Primary school	70	13.5
Junior high school	246	48.2
Senior high school/vocational high school/technical secondary school	101	19.5
College/Bachelor degree or above	53	10.5
Marital status		
Unmarried	80	15.5
Married	412	80.4
Widowed/Divorced	22	4.7
Average monthly income of whole family (yuan)		
< 500	19	3.9
500–999	3	0.8
1000–1999	15	2.9
2000–4999	199	38.8
5000–9999	181	35.4
≥ 10000	81	3.3
I don’t know	16	3.4
Occupation		
Person in charge of enterprises and institutions	16	3.4
Professional and technical personnel	90	17.5
Agricultural, forestry, animal husbandry and fishery production personnel	18	3.8
Commercial and service personnel	51	10.0
Production and transportation equipment operator	22	4.6
People		
Unemployed and laid-off workers	13	2.7
Migrant workers and others	300	58.9

The average monthly household income was primarily between 2000–4999 yuan (38.7%), followed by 5000–9999 yuan (35.2%). Occupation-wise, 58.8% were migrant workers, 17.7% were professionals, 10.0% worked in business and services, and the remaining 13.5% were engaged in other sectors. The demographic characteristics of respondents are summarized in **Table 1**.

The respondents who answered 80% or more of health literacy questionnaire correctly were identified as having health literacy. The proportion of floating population in many provinces in China with health literacy was 1.0%, and proportion with basic knowledge and concept literacy was 7.39%. The proportion of behavioral literacy was 0.78%, and proportion of basic skills literacy was 17.51%, see **Table 2**. Among floating population with health literacy, proportion of men is higher than that of women. Among 394 men, 4 people have health literacy, accounting for 1%, and proportion of women is 0.9%. Among ages, floating population between ages of 26 and 35 has highest proportion of health literacy, accounting for 2.8% of population at this stage. At same time, in basic knowledge and concepts, healthy lifestyle and behavior, proportion of population at this stage is It is also higher, at 9.3% and 1.8%, but among basic skills, proportion of floating population aged < 25 is 24.2%, slightly higher than that of floating population aged 26–35.

Table 2. The proportion of floating population with health literacy in Jinan.

Group	**Health literacy *n* (%)**	**Basic knowledge and concept (*n* %)**	**Healthy lifestyle and behavior *n* (%)**	**Basic skill *n* (%)**
Gender				
Male	4 (1.2)	31 (7.7)	3 (0.9)	59 (15.3)
Female	1 (0.8)	7 (6.2)	1 (0.8)	31 (26.3)
Age (years)				
≤ 26	0 (0)	4 (4.3)	1 (1.2)	24 (24.4)
27–36	3 (2.6)	10 (9.5)	2 (1.6)	26 (23.5)
37–46	1 (0.8)	11 (8.8)	1 (0.9)	20 (15.5)
47–56	1 (0.7)	11 (9.3)	0 (0)	12 (9.7)
57–70	0 (0)	2 (3.5)	0 (0)	8 (14.7)
Degree of education				
Illiterate or illiterate	0 (0)	0 (0)	0 (0)	2 (4.5)
Primary school	0 (0)	4 (4.4)	0 (0)	6 (8.8)
Junior high school	1 (0.5)	11 (4.5)	1 (0.5)	32 (13.1)
Senior high school/vocational high school/technical secondary school	3 (3.3)	17 (17.5)	3 (3.2)	25 (25.2)
College/Bachelor degree or above	1 (2.0)	7 (13.4)	0 (0)	25 (47.4)

The difference in proportion of men and women basically possessing health literacy is not very large, see **Table 3**; except for basic skill literacy, proportion of residents aged 56–69 who basically possess health literacy is significantly lower than that of floating population of other ages, see **Table 4**; In terms of educational level, higher education level, higher proportion of health literacy, see **Table 5**.

Table 3. Proportion of floating population of different genders with basic health literacy (%).

Entry	Female	Male	X^2	p
Health literacy	40 (34.4)	152 (38.6)	0.808	0.369
Basic knowledge and concept	38 (32.7)	184 (46.7)	7.664	0.005
Healthy lifestyle and skills	39 (32.6)	115 (29.3)	0.558	0.453
Basic skill	58 (48.9)	190 (48.4)	0.011	0.822

Table 4. Proportion of respondents of different ages with basic health literacy (%).

Entry	≤ 26	27–36	37–46	47–56	57–70	X^2	p
Health literacy	38 (39.4)	47 (43.2)	54 (42.5)	39 (32.4)	14 (25.6)	7.792	0.097
Basic knowledge and concept	38 (39.4)	49 (45.3)	60 (46.7)	57 (47.3)	18 (32.5)	4.719	0.316
Healthy lifestyle and skills	35 (35.6)	38 (34.3)	36 (28.4)	33 (27.5)	12 (21.6)	4.826	0.307
Basic skill	52 (53.7)	59 (53.5)	62 (48.5)	47 (38.6)	27 (49.4)	6.686	0.155

Table 5. The proportion of respondents with different educational levels basically possessing health literacy (%).

Entry	Illiterate or illiterate	Primary school	Junior high school	Senior high school/vocational high school/technical secondary school	College/Bachelor degree or above	X^2	p
Health literacy	4 (9.5)	10 (14.5)	87 (35.6)	58 (60.6)	33 (62.5)	66.316	< 0.001
Basic knowledge and concept	5 (11.8)	17 (24.4)	107 (43.7)	62 (64.5)	30 (56.5)	49.355	< 0.001
Healthy lifestyle and skills	5 (11.8)	8 (11.1)	44 (26.6)	47 (47.2)	28 (52.6)	46.433	< 0.001
Basic skill	12 (27.8)	21 (30.0)	108 (43.7)	67 (67.2)	39 (73.5)	46.033	< 0.001

The floating population in many provinces in China basically has literacy of five types of health problems also shows following characteristics: Proportion of men who have literacy of five types of health problems is slightly higher than that of women, as shown in **Table 5**. According to health literacy status of floating population in many provinces in China, this paper analyzes health literacy status and influencing factors of five types of health problems, including scientific health concept, infectious disease prevention, chronic disease prevention, safety and first aid, and basic medical care. The proportions of floating population in many provinces in China who basically have literacy of five types of health problems are ranked from high to low: Safety and first aid literacy 65.18%, scientific health concept literacy 60.7%, infectious disease prevention literacy 39.88%, basic medical literacy 26.85%, chronic disease literacy Prevention literacy 11.87%.

5. Experiments

The analysis shows that the overall system is greatly impacted by the performance of a single node. The following three aspects of this system are verified and assessed: Single node posture capture, sensor calibration, and sensor data analysis.

5.1. Analysis of accelerometer raw data

Accelerometers are mostly used to measure an object's velocity, however if the item is not stationary with regard to the earth, their noise level rises noticeably. The Y-axis sensor is positioned vertically up while sensor #2 is positioned horizontally. After a week of spinning around the Y-axis, the accelerometer's X-axis output is shown in **Figure 4**. Theoretically, the X-axis output should be zero when rotating around the Z-axis at a constant speed. However, because it is difficult to maintain perfect homogeneity during rotation, the X-axis adds extra acceleration.

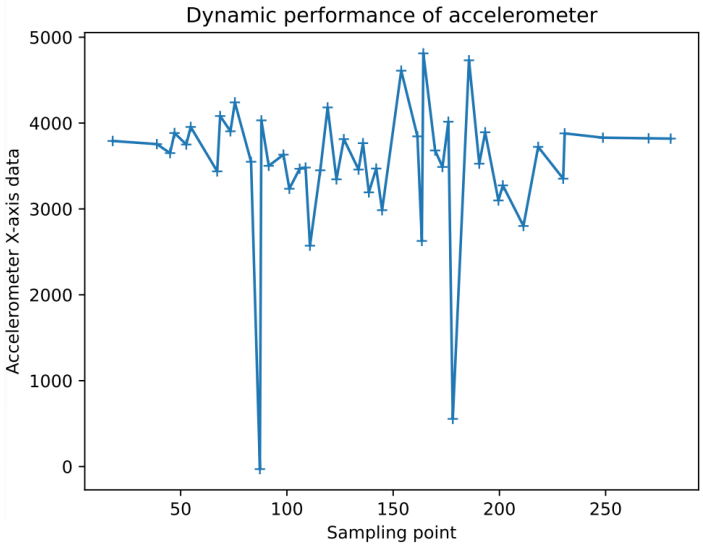

Figure 4. Noise in the accelerometer's dynamic case.

5.2. Examination of unprocessed gyroscope data

Mechanical, laser, and MEMS gyroscopes are commonly used in robotics and aerospace applications, each offering distinct advantages and limitations. Mechanical gyroscopes, while widely utilized in missile navigation systems due to their precision, are generally too large for applications that require compact designs. In contrast, laser gyroscopes offer a more affordable solution but are not well-suited for motion capture systems due to their size and complexity.

For this system, the MPU9250 integrated gyroscope is employed. This choice provides a balanced solution, offering a compact, reliable, and cost-effective option suitable for motion capture applications. The system is powered by a 3.7 V lithium battery, ensuring portability and ease of deployment. During the testing phase, the system is connected via a USB 3.0 interface for data transfer, providing fast communication between the sensor nodes and the processing unit.

The system operates with a sample frequency of 40 Hz, ensuring a sufficient data rate for capturing motion details. With an acquisition time of approximately 1 min, the data collection process is optimized to maintain stability in the chosen node while monitoring motion in all three axes. This setup enables precise motion tracking in dynamic environments, offering valuable insights for applications such as biomechanics, sports performance analysis, and rehabilitation monitoring.

Future improvements could focus on enhancing the sensor's data resolution and expanding the sampling frequency to further refine motion tracking capabilities, particularly for high-speed movements or complex dynamic scenarios.

As can be seen in **Figure 5**, the MEMS gyroscope suffers from high noise levels with some anomalous spikes. Direct integration of these data results in an increase in noise that accumulates over time. In addition to integration errors, gyroscopes are also affected by motion, temperature variations, and the phenomenon of drift. The slow departure of a gyroscope's output from zero at rest is known as drift. The gyroscope data were mean filtered with a filter window size of 25 to visualize the drift phenomenon. In just 1 min, the gyroscope drifted considerably in the negative direction, as shown in **Figure 6**. Even without integration error, the baseline drift increases the error in the integration result.

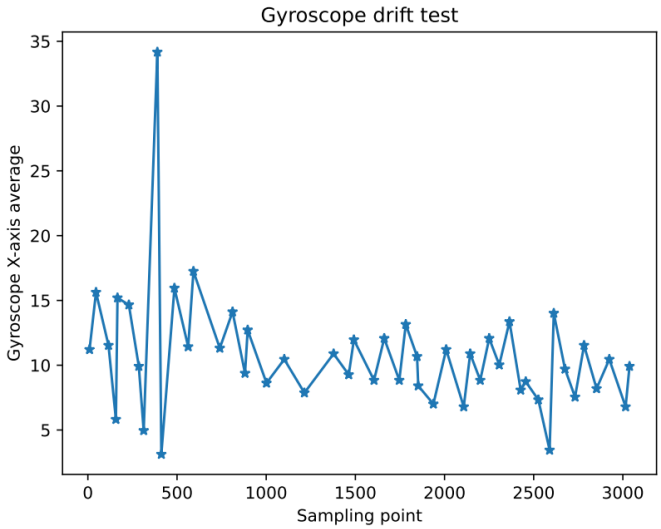

Figure 5. Test of gyroscope static drift.

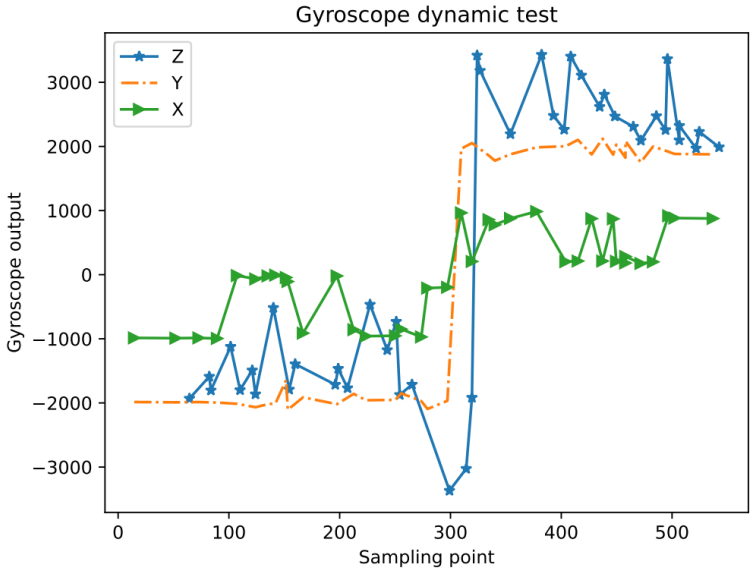

Figure 6. Dynamic gyroscope test.

5.3. Test of angle tracking

The final results are significantly impacted by whether or not geomagnetic timing is enabled, as shown in **Figure 7**. The heading angle inaccuracy in IMU mode increased over time when geomagnetic timing was not enabled, while it constantly fluctuated around 0 degrees when it was. Furthermore, the heading angle error in IMU mode rose linearly when geomagnetic timing was not enabled, suggesting that integration was the primary source of the problem. The heading angle inaccuracy would increase too quickly for the system without geomagnetic timing.

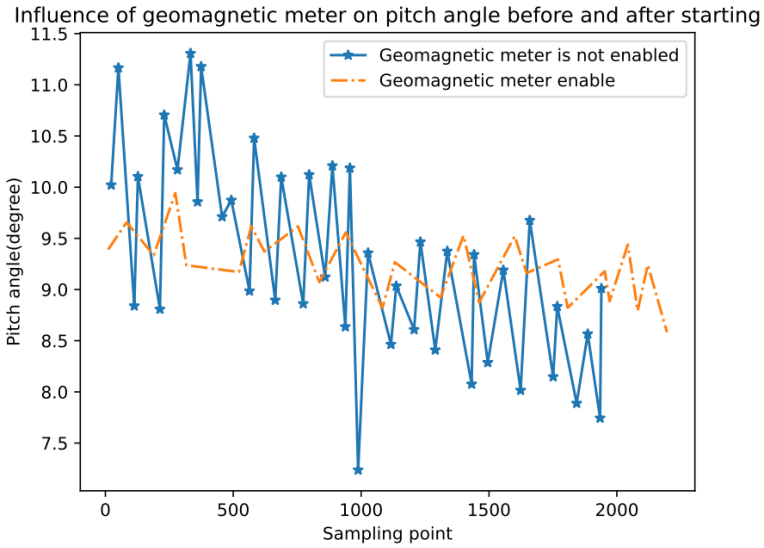

Figure 7. The geomagnetic meter's effect.

5.4. Check for motion capture of the entire body

Compared to single-node posture tracking, multi-node human motion capture introduces significantly greater complexity, as it involves simultaneous monitoring and synchronization of multiple sensors to achieve a comprehensive representation of body dynamics. While this study does not yet incorporate tracking of human body position, the current tests focus exclusively on capturing and analyzing full-body motion.

This approach prioritizes the monitoring of joint movements and limb coordination, enabling a detailed understanding of motion patterns without the added complexity of positional tracking. **Figure 8** illustrates the physical effects achieved through this full-body motion capture system, showcasing its ability to accurately capture intricate motion sequences and deliver high-fidelity biomechanical data.

Future enhancements may integrate position tracking to provide a holistic view of human movement, further expanding the system's applicability in areas such as ergonomics, virtual reality, and advanced sports performance analysis. For now, the emphasis on motion rather than position ensures optimized accuracy and streamlined functionality, making the system a practical and reliable tool for various biomechanical applications.

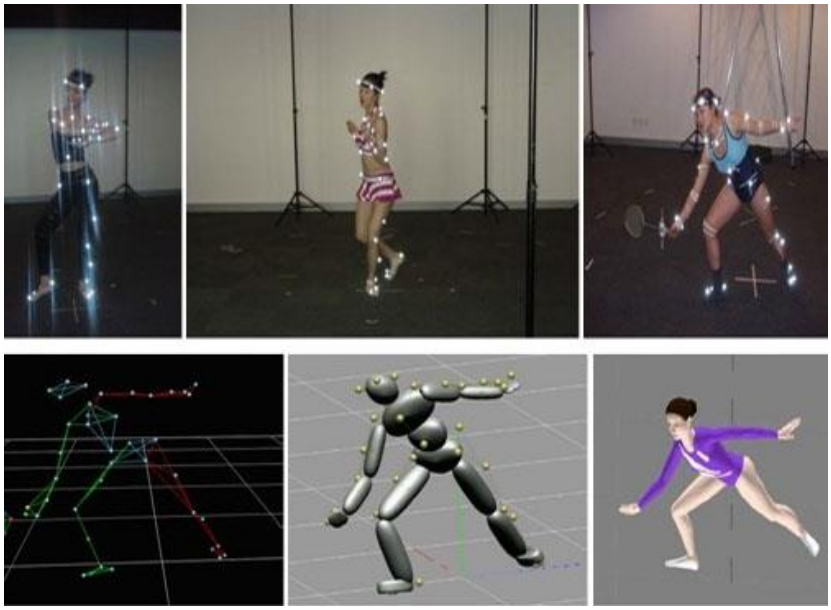

Figure 8. The mobility of the entire body.

It is rather simple for subjects to calibrate the device; they only need to stand and push the calibration button on the software interface. For calibration, the dorsal node must be in the center, while this is not strictly required. **Figure 8**, which shows five real-world movements at the top and screenshots of the relevant model motions at the bottom, demonstrates the impact of full-body motion capture. The picture shows how the system could capture the basic movements of the human body. The system contains 10 nodes, which makes the model movements a little stiff, thus there is still a difference between the system and the real-life model. For example, it is difficult for the system to fully represent and capture human gestures such as bending over. To improve the realism of the presentation in real-world applications, the model skeleton can also be adjusted to match the length of the human skeleton.

6. Conclusion

This study introduces an innovative, lightweight, multi-node IMU-based motion capture system designed to deliver a cost-effective and scalable solution for advanced biomechanical applications. By employing cutting-edge sensor calibration techniques and an enhanced Madgwick-based data fusion algorithm, the system achieves significant improvements in accuracy by effectively mitigating sensor drift, noise, and environmental interferences. These advancements enable precise, real-time motion tracking, catering to diverse applications such as gait analysis, sports performance evaluation, and rehabilitation monitoring.

The system's multi-node design ensures comprehensive coverage of human movement, while its lightweight and portable configuration enhances usability in dynamic and field-based environments. Supported by high-throughput USB 3.0 communication, the system delivers low-latency data transmission, ensuring seamless integration into real-time biomechanical workflows.

Experimental validation demonstrates the system's robustness and adaptability in capturing intricate motion patterns, even under challenging conditions. This makes

it an indispensable tool for biomechanics research, offering practical solutions for sports training optimization, injury prevention, and personalized rehabilitation strategies.

Moreover, the system’s affordability and ease of deployment hold promise for broad adoption across healthcare, sports science, and academic research. Its potential extends beyond biomechanics, paving the way for applications in ergonomics, elderly care, and remote health monitoring. This work represents a significant step forward in advancing motion capture technology and its applications in multidisciplinary fields.

Author contributions: Conceptualization, HM and XM; methodology, XM; software, HM; validation, HM and XM; formal analysis, XM; investigation, XM; resources, HM; data curation, HM; writing—original draft preparation, XM; writing—review and editing, HM; visualization, HM; supervision, XM; project administration, HM; funding acquisition, HM. All authors have read and agreed to the published version of the manuscript.

Ethical approval: Not applicable.

Conflict of interest: The authors declare no conflict of interest.

References

1. Lerma, N., and Gulgin, H. (2022). Agreement of a Portable Motion Capture System to Analyze Movement Skills in Children. Measurement in Physical Education and Exercise Science, 1–9.
2. Li, H., Cui, C., and Jiang, S. (2022). Strategy for improving the football teaching quality by AI and metaverse-empowered in mobile internet environment. Wireless Networks, 1–10.
3. Wang, T. J. (2022). A study on utilizing 3D motion-capture analysis to assist in Chinese opera teaching. Research in Dance Education, 23(2), 194–222.
4. Pilati, F., Faccio, M., Gamberi, M., and Regattieri, A. (2020). Learning manual assembly through real-time motion capture for operator training with augmented reality. Procedia Manufacturing, 45, 189–195.
5. Rout, A., Mahanta, G. B., Biswal, B. B., Vardhan Raj, S., and BBVL, D. (2024). Application of fuzzy logic in multi-sensor-based health service robot for condition monitoring during pandemic situations. Robotic Intelligence and Automation.
6. Dong, H. C., Liu, S., Pang, L. L., Tao, Z. G., Fang, L. D., Zhang, Z. H., and Li, X. T. (2023). A multi-sensor-based distributed real-time measurement system for glacier deformation. Journal of Mountain Science, 20(10), 2913–2927.
7. Arufe-Giráldez, V., Sanmiguel-Rodríguez, A., Ramos-Álvarez, O., and Navarro-Patón, R. (2023). News of the Pedagogical Models in Physical Education—A Quick Review. International Journal of Environmental Research and Public Health, 20(3), 2586.
8. Wu, Y. (2024). Exploration of the Integration and Application of the Modern New Chinese Style Interior Design. International Journal for Housing Science and Its Applications, 45(2), 28–36.
9. Wang, W. (2024). Esg Performance on the Financing Cost of A-Share Listed Companies and an Empirical Study. International Journal for Housing Science and Its Applications, 45(2), 1–7.
10. Goodyear, V. A., Skinner, B., McKeever, J., and Griffiths, M. (2023). The influence of online physical activity interventions on children and young people’s engagement with physical activity: A systematic review. Physical Education and Sport Pedagogy, 28(1), 94–108.
11. Luo, X., Zhang, C., and Bai, L. (2023). A fixed clustering protocol based on random relay strategy for EHWSN. Digital Communications and Networks, 9(1), 90–100.
12. Hernández-Mustieles, M. A., Lima-Carmona, Y. E., Pacheco-Ramírez, M. A., Mendoza-Armenta, A. A., Romero-Gómez, J. E., Cruz-Gómez, C. F., ... and Lozoya-Santos, J. D. J. (2024). Wearable Biosensor Technology in Education: A Systematic Review. Sensors, 24(8), 2437.

13. Yang, L., Amin, O., and Shihada, B. (2024). Intelligent wearable systems: Opportunities and challenges in health and sports. ACM Computing Surveys, 56(7), 1–42.
14. Alagdeve, V., Pradhan, R. K., Manikandan, R., Sivaraman, P., Kavitha, S., and Kalathil, S. (2024). Advances in Wearable Sensors for Real-Time Internet of things based Biomechanical Analysis in High-Performance Sports. Journal of Intelligent Systems & Internet of Things, 13(2).
15. Seçkin, A. Ç., Ateş, B., and Seçkin, M. (2023). Review on Wearable Technology in sports: Concepts, Challenges and opportunities. Applied Sciences, 13(18), 10399.